Nonadiabatic small polarons, positive magnetoresistance, and ferrimagnetism behavior in the partially inverse $Mn_{2-x}V_{1+x}O_4$ spinels

E. V. Pannunzio-Miner,[1] J. M. De Paoli,[2] R. E. Carbonio,[1] and R. D. Sánchez[2,a)]
[1]*INFIQC (CONICET), Departamento de Fisicoquímica, Facultad de Ciencias Químicas, Universidad Nacional de Córdoba, Ciudad Universitaria, 5000 Córdoba, Argentina*
[2]*Centro Atómico Bariloche, Comisión Nacional de Energía Atómica, 8400 Bariloche, Argentina*

(Received 13 November 2008; accepted 26 March 2009; published online 2 June 2009)

We present experimental results of electrical resistivity (ρ), magnetoresistance (MR), Seebeck coefficient (S), and magnetic susceptibility (χ) experiments at high temperature on the spinel $Mn_{2-x}V_{1+x}O_4$ series with $x=0$, $\frac{1}{3}$, and 1, prepared by solid state reaction. The Rietveld analysis of neutron powder diffraction (NPD) patterns confirm the expected cubic symmetry (SG: Fd-$3m$) with cell parameters around 8.5 Å. We also precisely calculate the distribution of Mn/V cations, in the tetrahedral and octahedral sites, for the whole series showing an important degree of inversion. The magnetic susceptibility and electrical transport properties show ferrimagnetic and semiconductor behaviors, respectively. A large difference detected between the activation energies for S and ρ indicates the presence of small polarons and the temperature dependence of ρ is well fitted with the nonadiabatic polarons model. All the samples present positive MR at room temperature, in particular, the highest value (around 1%) was observed in the MnV_2O_4 sample. © *2009 American Institute of Physics*. [DOI: 10.1063/1.3124361]

I. INTRODUCTION

Since the discovery of the colossal magnetoresistance (CMR) phenomenon[1,2] more than a decade ago, the interest of many researchers has been focused on the basic physic problems and also on the possible technological applications.[3,4] The principal reasons to study manganites are the fascinating scenery where the orbital, charge, lattice, and spin are degrees of freedom that can interact between them.[5] In particular, their interplay in some special conditions of magnetic field, temperature, pressure doping, etc., leads to a phase separation phenomenon where an insulator (I) antiferromagnetic (AFM), or I with charge order, phase coexists with a metallic (M) and ferromagnetic (FM) one.[6] More interesting is the coexistence of phases around the Curie temperature in $La_{0.67}Ca_{0.33}MnO_3$, where the CMR effect is maximized and it has been explained by the coexistence of the M-FM phase with an I phase where the electric transport is dominated by a polaronic state.[7] Indeed, the interaction between spins and lattice takes a relevant importance to describe more realistically the phenomena observed in these systems.[8] On the other hand, the difference between the activation energy obtained from the resistivity and that obtained from thermopower experiments is also an indication of a carrier-lattice interaction, which is normally associated with the presence of small polarons in the system.[9]

The spinels are a family of materials with a renewed interest by several contact points with the manganite systems. Recent theoretical work shows a debate about the origin of the complex nature where there is a competition between several degrees of freedom as spin, orbital order, and lattice.[10–13]

The oxygen ions form a cubic close-packed arrangement in the spinel crystal structure with general formula AB_2O_4. The metallic A ions are surrounded by four oxygen atoms at the vertices of a tetrahedrom, while the metallic B atoms are surrounded by six oxygen at the vertices of an octahedrom. As the spinel formula indicates, the tetrahedral and octahedral sites are two nonequivalent types of crystallographic sites with a ratio 1:2 and these are generally called A and B sublattices, respectively.

Several spinels, with magnetic ions occupying only one sublattice (A or B), are geometrically frustrated materials. It is possible to observe an important difference between T_N (the temperature where normally occur the magnetic large range order–LRO), and θ. The θ/T_N ratio is taken as the magnetic frustration degree. Below T_N, some authors observed the coexistence between LRO and SRO (short range order) regions using special techniques as inelastic neutron dispersion and muon spin relaxation.[14] The ground state can be a spin-glass-like, where the more common signatures are the hysteresis and difference between field-cooling (FC) and zero-field cooling (ZFC). Also, other special and not common ground states can be the called spin-liquids and spin ices states.[14]

However, in the particular AV_2O_4 case, with nonmagnetic 2+ ions A=Zn, Mg, and Cd, the V^{3+}-ions (in the B sites) form a pyrochlore lattice. This type of lattice introduces a geometric frustration inherent to the structure, but part of this magnetic frustration can be removed by the ordering of orbitals, which explains the observed AFM structure.[15,16] On the other hand, if the A site is occupied by a magnetic ions as Mn^{2+}, a $3d^5$ high spin configuration $S=\frac{5}{2}$ with quenched orbital angular momentum and the B site with a nonmagnetic ion (as Al^{3+}), below 40 K AFM order is also observed.[17]

More complicated spinels, from a magnetic point of

a)Author to whom correspondence should be addressed. Mailing address: Rodolfo D. Sánchez, Centro Atómico Bariloche, 8400 Bariloche, Río Negro, Argentina. Tel.: +54-2944-445158. FAX: +54-2944-445299. Electronic mail: rodo@cab.cnea.gov.ar.

TABLE I. Data of Mn/V occupancies in the spinel structure ($Mn_{2-x}V_{1+x}O_4$) were obtained by Rietveld refinement of NPD data (Ref. 21). Ions between brackets are in octahedral sites. a is the cell parameter of the cubic spinel and the ionic model is the one that best describes the fit of Fig. 2.

x	Refined occupancies	a (Å)	Model I	Model II
0	$Mn_{0.89}V_{0.11}[Mn_{1.11}V_{0.89}]O_4$	8.5276(2)	$Mn^{2+}{}_{0.89}V^{4+}{}_{0.11}[Mn^{2+}{}_{1.11}V^{4+}{}_{0.89}]O_4$	$Mn^{2+}{}_{0.89}V^{3+}{}_{0.11}[Mn^{3+}{}_{1.11}Mn^{2+}{}_{0.11}V^{3+}{}_{0.89}]O_4$
$\frac{1}{3}$	$Mn_{1.00}[Mn_{0.67}V_{1.33}]O_4$	8.5617(1)	$Mn^{2+}{}_{1.00}[Mn^{2+}{}_{0.67}V^{3+}{}_{0.66}V^{4+}{}_{0.67}]O_4$	$Mn^{2+}{}_{1.00}[Mn^{3+}{}_{0.67}V^{3+}{}_{1.33}]O_4$
1	$Mn_{0.75}V_{0.25}[Mn_{0.25}V_{1.75}]O_4$	8.5849(2)	$Mn^{2+}{}_{0.75}V^{3+}{}_{0.25}[Mn^{2+}{}_{0.25}V^{3+}{}_{1.75}]O_4$	Idem model I

view, have magnetic ions in both spinel sites. Particularly, there has been an emerging interest with MnV_2O_4.[18,19] where the orbital-spin coupled system presents a switching of the crystal structure by magnetic field (magnetoelastic effects).[20] MnV_2O_4 is a normal spinel, which presents magnetic order at low temperature (T_N=56 K). The Mn^{2+} ions occupy 8 tetrahedral (A) sites and the V^{3+} ions are in 16 octahedral (B) sites. Each V has six neighbors and the AFM interaction between them is dominant.

In general, in these kinds of spinels, where both nonequivalent sublattices are occupied with magnetic ions, the frustration is removed and ferrimagnetic order can be detected due to the nonequivalent crystallographic sites. However, due to the geometrically frustrated characteristic of these materials, the change in some parameters as the replacement of B ions by other magnetic ions, or the interexchange of sites by the ions (inversion) can originate the presence of magnetic SRO regions in a wide temperature range. This effect can favor the formation of magnetic polarons, which can introduce important consequences in the magnetoresistance (MR).

In this sense, we replace the V by Mn in the well know MnV_2O_4, x=1 in the formula $Mn_{2-x}V_{1+x}O_4$, precisely with $x=\frac{1}{3}$ and x=0 in order to study how it affects the transport and magnetic properties. We found that our samples also present a complex degree of occupation of the A and B sites by the Mn and V ions. We found a difference between the activation energies obtained from ρ and S, respectively. Also we show that the conduction mechanism is mediated by nonadiabatic small polarons and an important positive MR is even observed at room temperature (RT) for all the compositions. From a magnetic point of view, the samples present magnetic order (below approximately 56 K) and the temperature dependence of the inverse of the magnetic susceptibility clearly shows ferrimagnetic behavior.

II. EXPERIMENTAL

The samples were prepared by solid state reaction in sealed evacuated quartz ampoules heated several times (with intermediate regrinding) during periods of 12 h at 1000 °C and slowly cooled to RT. For each of the samples we found the best conditions of synthesis to be: for x=0 three times, for $x=\frac{1}{3}$ one time, and for x=1 two times plus one treatment under Ar(95%) H_2(5%). The cubic structure Fd-3m at RT was confirmed by NPD and the lattice parameter (a) was obtained from the Rietveld refinement showing that a increases, as it is expected, with the Mn content in the spinel. The lattice parameter at RT of each spinel is indicated in Table I. From the analysis of the patterns, the Rietveld refinement also shows the distribution of cations in the tetrahedral and octahedral sites. The fact that both ions (Mn and V) are distributed in both crystallographic sites ($Mn_aV_b[Mn_cV_d]_2O_4$) indicates that these oxides are partially inverse spinels. The details of the refinements are discussed by the authors in another publication.[21]

The dc magnetization was measured with a commercial superconducting quantum interference device (SQUID) magnetometer on powdered samples, in the temperature range of 5–300 K and H up to 50 kOe. From RT to 700 K a home-made Faraday balance was used.

The electrical resistivity was measured using four probes method in a commercial cryostat applying magnetic fields (H) up to 50 kOe and a current of 1 μA parallel to H (longitudinal configuration). The probes were welded with silver paint on sputtered gold electrodes on the sintered pellets. The Seebeck coefficient was measured in a home-made device with temperature gradients of $\pm$1.5 K. Both experiments only were performed in the short temperature range between 200 and 300 K due to the high resistance reached (tens of megaohms).

III. RESULTS AND DISCUSSION

A. Magnetic properties

For the ZFC experiments, the sample was cooled from 300 K with H=0; afterwards, an H=5 kOe was applied and the magnetization (M) data were collected increasing T. Field cool cooling (FCC) was performed by cooling the sample with H=5 kOe measuring M. On the right panels of Fig. 1, we show the details of M(ZFC) and M(FCC) magnetization data as a function of T, taken at 5 kOe. We determine the order temperature (T_N) as the minimum value in the dM/dT versus T curve, obtaining 42, 52, and 58 K for x =0, 1/3, and 1, respectively.

At low temperature an important difference between both curves is only observed in the x=1 sample. This difference can be an indication of the important magnetic frustrations present in the system. Although, recently, this system has been extensively studied and some authors found a second order transition (T_N=57 K) from a paramagnetic to ferrimagnetic (collinear ordering). An extra first order transition at slightly lower temperature associated with the orbital order of the V ions and the ferrimagnetic order becomes in a noncollinear state where the V spins developing AFM components in the ab plane.[22] The magnetic state of this spinel is today under discussion.

On the left panels of Fig. 1, the hysteresis loops at 5 K

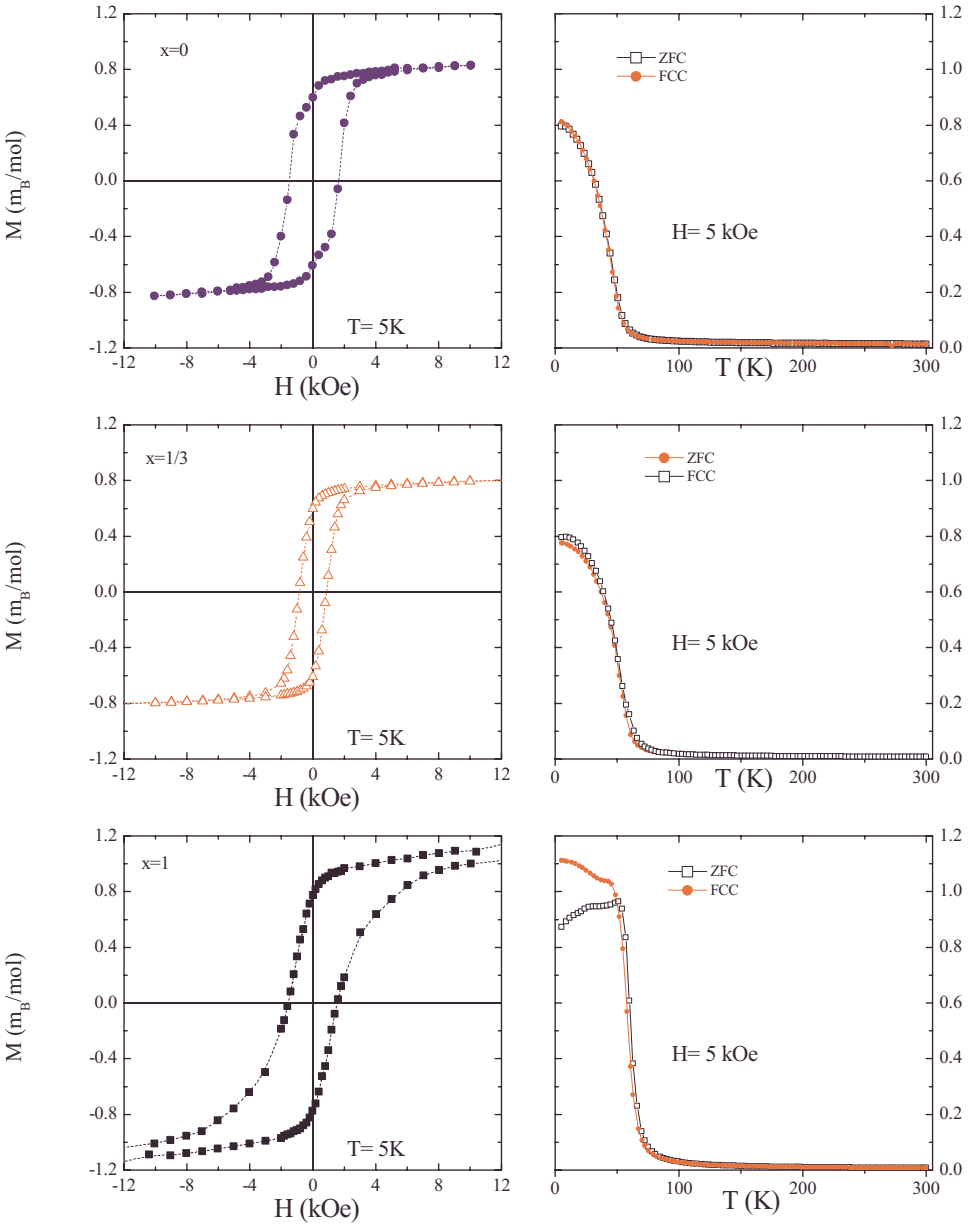

FIG. 1. (Color online) For $Mn_{2-x}V_{1+x}O_4$ (with $x=0$, $\frac{1}{3}$, and 1), left panels show M vs H at 5 K and right panels represent M(ZFC) and M(FC) both measured at 5 kOe and as a function of T.

and up to 10 kOe are shown for all the samples. Important coercive values, between 1 and 2 kOe, are observed in the three samples. The maximum values of magnetization obtained at low temperature for $x=0$, 1/3, and 1 are 0.9, 0.8, and 1.1 μ_B/mol, respectively. In particular, the maximum value for $x=1$ is less than the values reported by previous authors and the 2.08 μ_B/mol obtained by us from neutrons diffraction experiments.[21] The fact that the magnetic moment saturation is not completely reached, the shape of the magnetization and demagnetization branches and the differences between the ZFC and FCC curves, suggests that some magnetic clusters are present in this system at low temperature. It could be a consequence of the high inversion degree that present these spinels in powder and prepared with the present method. On the other hand, some consideration should be taken into account to compare with a theoretical prediction as that the V^{3+} is partially orbital quenched (1.4 μB), covalence and crystal field effects, the distribution of the magnetic ions over the two sublattices, the valence of the ions can be variable and sublattice magnetization may be triangular or other spin arrangement. In the next paragraphs, we will focus our attention in the high temperature behavior of these spinels.

The χ data were computed as the ratio between M and H. In all the samples, we subtracted the holder contribution and diamagnetic core contributions ($\chi_{\text{diamag}} \cong -8.3 \times 10^{-5}$ emu/mole). In Fig. 2 we show the temperature dependence of the inverse of magnetic susceptibility (χ^{-1}) for $x=0$, $\frac{1}{3}$, and 1, respectively. At high T the curves present a linear behavior but these drops drastically close to T_N. This behavior is typical of ferrimagnetic materials as it is expected in the spinels. Between $400 < T(\text{K}) < 700$, χ^{-1} presents an asymptotic tendency to a Curie–Weiss law (see Table II).

Above T_N, using the molecular field theory of the ferrimagnetism, the equation that describes a hyperbola of χ^{-1} is

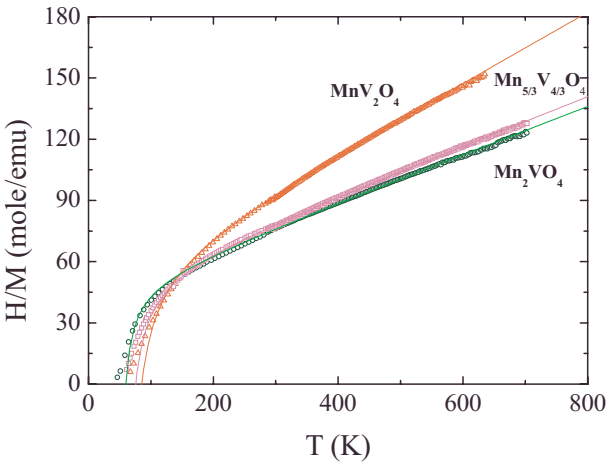

FIG. 2. (Color online) χ^{-1} vs T for $Mn_{2-x}V_{1+x}O_4$. The symbols are the experimental data and the lines are the expected paramagnetic behavior for a ferrimagnet, which can be described by a mean field model. Note the excellent agreement with the experimental data.

$$\frac{1}{\chi} = \frac{T}{C} - \frac{1}{\chi_0} - \frac{\sigma}{T-\theta'}, \tag{1}$$

where χ_0 is the ratio between C (the Curie–Weiss constant) and θ ($\chi_0 = C/\theta$), σ is an experimental mean field parameter, and θ' is an experimental temperature, which should be equal or greater than T_N. We fit the experimental data with Eq. (1).

To calculate the Curie–Weiss constants (C) expected for these ferrimagnetic spinels, we considered the ions occupancies (a, b, $2c$, and $2d$) obtained from NPD refinements (Table I and details in Ref. 21), according to the spinel chemical formula $(Mn_aV_b[Mn_cV_d]_2O_4)$. Also, in Table I we show five feasible ionic configurations that can be considered to explain the magnetic and electric behaviors of these three studied spinels. The choice of these configurations is based on thermodynamic considerations and charge conservation. These arguments are explained in detail in Ref. 21. We considered that essentially no V^{2+} spinel are reported in the literature and V^{5+} and Mn^{4+} are too oxidized ions for our reducing synthetic conditions in order to discard configurations that include these ions. The result of the Curie–Weiss constants for each feasible case considered has been computed adding the individual ionic contribution of the $3d$ involved ions as $C = aC(Mn^{2+}) + bC(V^{3+}) + b'C(V^{4+}) + 2cC(Mn^{2+}) + 2c'C(Mn^{3+}) + 2dC(V^{3+}) + 2d'C(V^{4+})$. Note that some stoichiometric coefficients (b, b', c, c', d, or d') can be null, depending of the case (see Table I) and each C ($3d^n$) has the square magnetic moment modulus information and it tends to differentiate the Curie constant more markedly between the proposed models. The calculated C values for each feasible model explained in Table I are shown in Table II. The results of the fits curves using Eq. (1) can be observed with solid lines in Fig. 2 and the parameters are also shown in Table II. Comparing the C values obtained from the fits with those C values calculated from the feasible ionic models, we propose that the more adequate ionic models that describe the magnetic properties are

$$Mn^{2+}_{0.89}V^{3+}_{0.11}[Mn^{3+}_{1.11}Mn^{2+}_{0.11}V^{3+}_{0.89}]O_4,$$

$$Mn^{2+}_{1.00}[Mn^{2+}_{0.67}V^{3+}_{0.66}V^{4+}_{0.67}]O_4,$$

$$Mn^{2+}_{0.75}V^{3+}_{0.25}[Mn^{2+}_{0.25}V^{3+}_{1.75}]O_4. \tag{2}$$

For $x = 0$, $\frac{1}{3}$, and 1, respectively.

TABLE II. Magnetic and transport parameters obtained for different models and fitting of experimental data for the spinels $Mn_{2-x}V_{1+x}O_4$ (x=0, $\frac{1}{3}$, and 1). Models I and II are described in Table I. The bold values are the closer to the experimental value and the values with asterisks are the same because we use the same formula in both models.

Parameters	Mn_2VO_4	$Mn_{5/3}V_{4/3}O_4$	MnV_2O_4
x in $Mn_{2-x}V_{1+x}O_4$	0	$\frac{1}{3}$	1
	Magnetic data		
T_N (K)	46	52	58
C(emu/kmol) model I	10.4	**8.2**	**6.4***
C(emu/kmol) model II	**8.4**	6.4	**6.4***
C(emu/kmol) [Eq. (1)]	**8.56(3)**	**8.42(3)**	**5.87(2)**
$1/\chi_0 = \theta/C$(mol/emu) [Eq. (1)]	−43	−47	−48
θ (K)	−372	−399	−282
σ(kmol/emu) [Eq. (1)]	675(30)	1200(50)	1690(25)
θ' (K) [Eq. (1)]	43	52	58
	Transport		
E_ρ (meV) [ln ρ vs $1/T$]	290	190	300
c (carrier concentration)	0.445	0.335	0.125
$S_\infty(\mu V/K)$	–25	119	227
$S_\infty(\mu V/K)$-experiment	−36	25	60
E_S (meV)	20	21	18
E_ρ (meV) (nonadiabatic small polarons model)	230	180	240

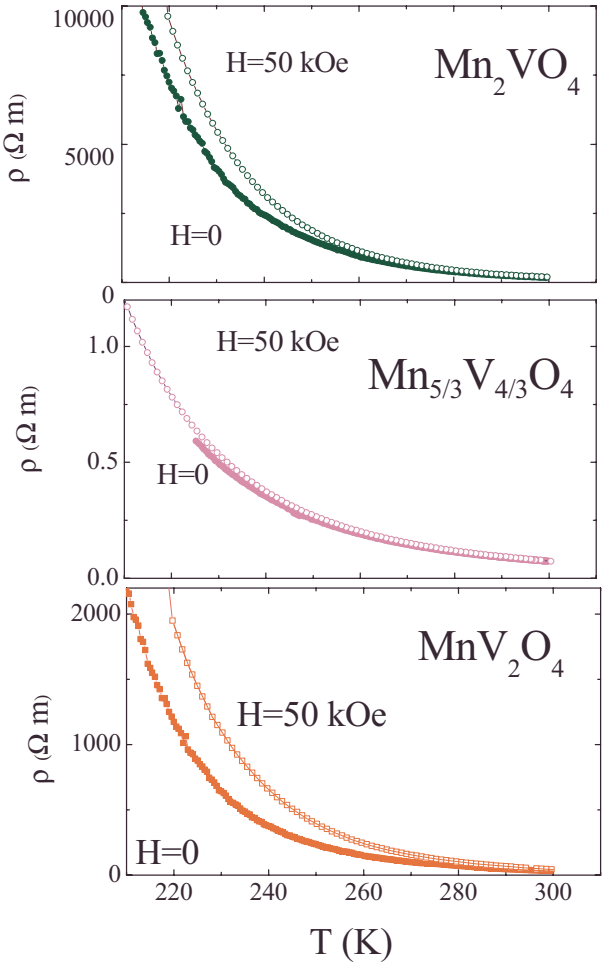

FIG. 3. (Color online) Electrical resistivity of $Mn_{2-x}V_{1+x}O_4$ series at $H=0$ and 50 kOe as a function of temperature.

On the other hand, to obtain information from the theta values about the interaction between the involved ions is a complex task. Because, the samples present some degree of inversion and four magnetic species (Mn^{2+}, Mn^{3+}, V^{3+}, and V^{4+}), a total of ten different interactions, and ten mean field equations should be considered in the system, 3*A*-*A*, 3*B*-*B* and 4*A*-*B*, which is an excessive large number of adjustable parameters and does a little confidence in the validity of the meaning of theta values. Anyway, the best fit of the experimental data with a hyperbola equation shows that these spinels present essentially AFM interaction between both sublattices and these oxides tend to a ferrimagnetic order at low temperatures.

B. Electrical properties

In Fig. 3 we show ρ versus T for the $x=1$, $\frac{1}{3}$, and 0 samples at $H=0$ and $H=50$ kOe respectively. The resistivity increases when the temperature is decreased for all the cases. The collected $\rho(H)$ values, when a magnetic field is applied, are larger than those taken in absence of magnetic field $\rho(0)$ data, resulting in a positive MR. The MR is computed as $\rho(H)$-$\rho(0)/\rho(0)$ and for the $x=1$ case at $H=50$ kOe, in the paramagnetic phase, reaches around 35% at 220 K, and approximately 1.5% at RT (see Fig. 4). For other samples, i.e., with $x=0$ and $\frac{1}{3}$ also we observe similar behavior but the MR values are below this limit.

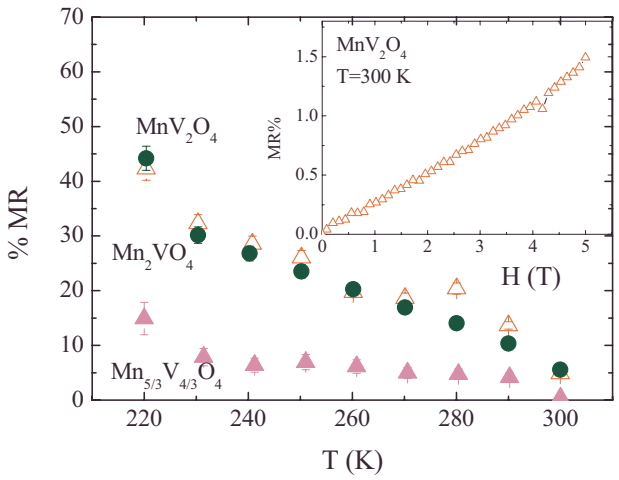

FIG. 4. (Color online) Percentage of MR as a function of temperature for $Mn_{2-x}V_{1+x}O_4$ (with $x=0$, $\frac{1}{3}$, and 1). Inset: we only show %MR vs H data at RT for MnV_2O_4.

In Fig. 5, ln ρ versus T^{-1} is plotted for $x=0$, $\frac{1}{3}$, and 1 samples. All of them can be described reasonably by a semiconducting behavior, $\rho=\rho_0 e^{E\rho/k_B T}$, where E_ρ should be the gap between bands. Although some small deviations of the linear behavior can be appreciated, the behavior corroborates at least that all the samples are semiconductors and present a thermal activation mechanism. We call the attention that the sample with $x=\frac{1}{3}$ presents the lower resistivity ($\rho \approx 0.076$ Ω m) compared to the end members of the series. We calculated E_ρ from the slope of the curves in Fig. 6 and we obtained $E_\rho=290$, 190, and 300 meV for the $x=0$, $\frac{1}{3}$, and 1 samples, respectively. Note that the ionic model proposed for the sample with $x=\frac{1}{3}$ is the only one that has a mixture of different vanadium species; this should facilitate the conduction across the t_{2g} orbitals.

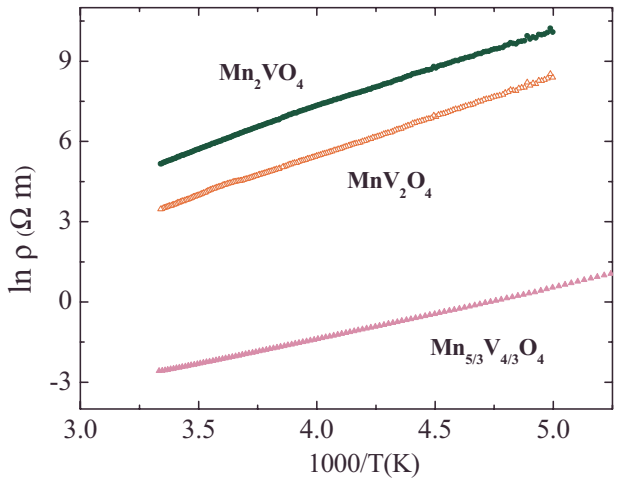

FIG. 5. (Color online) ln ρ vs $1000/T$ for $Mn_{2-x}V_{1+x}O_4$ samples with $x=0$, $\frac{1}{3}$, and 1. The plot shows that some thermal activated mechanism is present in the systems.

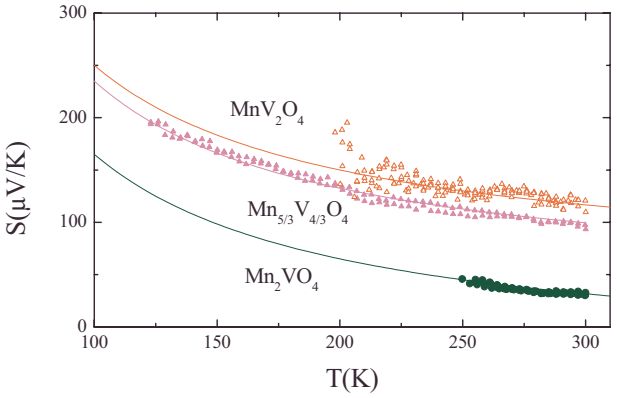

FIG. 6. (Color online) Seebeck coefficient as a function of temperature for $x=0$, $\frac{1}{3}$, and 1 samples. The solid lines represent the fit of the experimental data with a semiconductor behavior as given by Eq. (5).

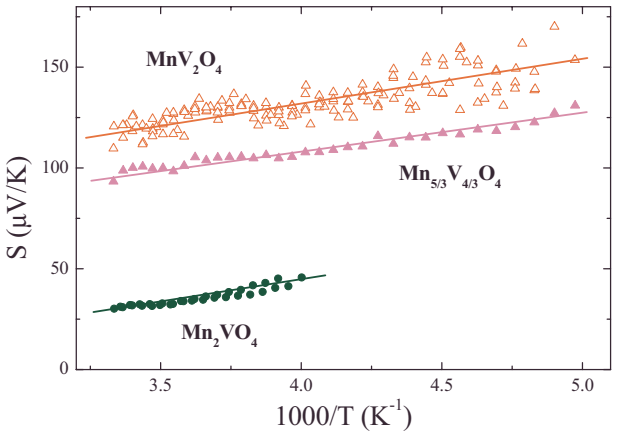

FIG. 7. (Color online) Seebeck coefficient as a function of $1000/T$ for $x=0$, $\frac{1}{3}$, and 1 samples. The solid lines represent linear fits of the experimental data.

In order to explore with more detail the transport mechanism involved in this system, we also measured the S coefficient in the series. The Seebeck of semiconducting materials is described by

$$S = \frac{k_B}{e}\left[\ln\left(\frac{N}{n}\right) + E\right], \tag{3}$$

where S_∞ is an entropy term, which is a constant, n is the carrier concentration, which is temperature dependent for semiconductors with a thermally activated dependence, and N is the limiting value of n expressed by

$$n = N\exp\left(\frac{E_S}{k_B T}\right). \tag{4}$$

Introducing Eq. (4) in Eq. (3), the Sebeeck (S) for semiconducting materials is

$$S = \frac{k_B}{e}\left[\frac{E_S}{k_B T} + S_\infty\right], \tag{5}$$

where E_S is the Seebeck band gap and S_∞ is the asymptotic value at high temperature and it includes the spin[23] and configurational[24] entropies of the carriers. The experimental values obtained from the fitted curves are in Table II. Normally, the contribution to S due to the spin configuration has the form

$$S_\sigma = \frac{k_B}{e}\ln\left[\frac{2\sigma+1}{2\sigma_0+1}\right], \tag{6}$$

where σ and σ_0 are the spin of the involved species in the conduction. While, in general, the configurational term adopts the Heikes formula,

$$S_c = \frac{k_B}{e}\ln\left[\frac{1-c}{c}\right]. \tag{7}$$

In spinels, electronic conduction takes place through octahedral sites, involving mainly t_{2g} orbitals, since they can directly overlap each other.[25] Consequently in order to calculate σ and σ_0 spin configurations, we use only the species present in the O sites that we discussed in the precedent magnetic section, in which we present the more feasible models. For example we have, for $x=0$, Mn_2VO_4, that the octahedral sites are occupied by $[Mn^{3+}_{1.11}Mn^{2+}_{0.11}V^{3+}_{0.89}]$ in our samples. We can think of this situation as a background of Mn^{3+} (and Mn^{2+}) ions with complete t_{2g}^3 configuration and acceptor centers of V^{3+} (t_{2g}^2). The carrier concentration of the t_{2g}^2 is $c=0.445$ and we can calculate S_c using Eq. (7) and from Eq. (6), $S_\sigma=-44\ \mu V/K$. Adding both contributions we have that $S_\infty \approx -25\ \mu V/K$ is very close to the $-36\ \mu V/K$ value obtained from the experiment. For the $x=\frac{1}{3}$ case, $Mn_{5/3}V_{4/3}O_4$, the octahedral sites are occupied by $[Mn^{2+}_{0.67}V^{3+}_{0.66}V^{4+}_{0.67}]$. This situation is very different because in this case the background is formed by V^{3+} and V^{4+} (t_{2g}^2 and t_{2g}^1) and the donors centers are Mn^{2+} ions ($c=0.335$) with t_{2g}^3 configuration and with an extra electron. We obtained $S_\sigma=59\ \mu V/K$ and consequently $S_\infty \approx 119\ \mu V/K$; $25\ \mu V/K$ is the experimental value. Finally, the $x=1$ sample with formula MnV_2O_4 which octahedral part is $[Mn^{2+}_{0.25}V^{3+}_{1.75}]$. The background is also the majority t_{2g}^2 coming from the d^2 (V^{3+}) and the donors t_{2g}^3 centers come from d^5 (Mn^{2+}). In this case, $c=0.125$ and $S_\sigma \approx 60\ \mu V/K$ being the calculated and experimental values of S_∞, 227 and $60\ \mu V/K$, respectively (See Table II). Although in the $x=\frac{1}{3}$ and $x=1$ cases, comparing the calculated values with those obtained with the fit of the Fig. 6 data, we find a factor of 4 of discrepancy, but the sign and the tendency of the Seebeck are in the correct direction. S_∞ values increase with x; for the $x=0$ sample we predict a negative value of S_∞, indicating conduction by holes, whereas for $x=\frac{1}{3}$ and 1 have positive S_∞ values, indicating conduction by electrons. This picture and the proposed ionic models are in good agreement with the data obtained from the experiments.

To corroborate the semiconducting behavior in this spinels, we make a S versus T^{-1} plot (see Fig. 7). From the slope we obtain $E_S \approx 20$ meV for all the samples and it is interesting to note that $E_\rho \gg E_S$. This large difference between the values of the activation energies, in the frame of strong electron-phonon coupling, has been interpreted as the formation of small lattice polarons.

The polarons are particles formed by interactions between electrons and the lattice; the carriers can jump (depending of the transfer integral) to the neighbors and are trapped during a certain time around a lattice deformation.

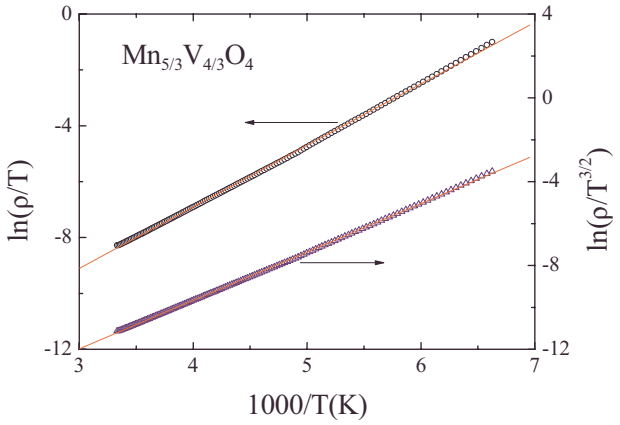

FIG. 8. (Color online) Polaron mechanisms: left $\ln(\rho/T)$ "adiabatic" and right $\ln(\rho/T^{3/2})$ "nonadiabatic." Both mechanisms are plotted as a function of $1000/T$. The lines are linear fits of the data and the best one (correlation coefficient close to 1) corresponds to the nonadiabatic polaron model.

When the lattice deformation is less or comparable to interatomic separation, these particles are called "small polaron." This idea was invoked to explain the transport properties in simple oxide as CoO or MnO,[26] manganites,[23,9,27] Ruddlesden Popper phases,[28] and spinels.[29] Thus, the energy gap obtained from the electrical resistivity is written as $E_\rho = E_S + W_H$, where W_H is the energy barrier that the polarons must surpass in order to hop to another site.[9,28] Therefore, the band gap of S in this regime is insensitive to polaron parameters, as for example, the size or the effective mass (that generates the barrier W_H). In this case W_H is approximately 180 meV. E_ρ is known as the activation energy for hopping.

At low temperatures ($T \ll \theta_D/2 - 200$ K), where θ_D is the Debye temperature of the oxide; the small polaron hopping between two sites occurs via quantum tunneling. While at high temperature ($T \geq \theta_D/2$, our experimental range) the small polarons have a thermally activated mechanism and the ρ of the system should be described by Eq. (8). The temperature exponent (α) of the pre-exponential term relates two different situations, which are envisaged for small polaron mobility. In the adiabatic limit ($\alpha=1$), which was deduced by Bosman and van Daal[26] and Emin and co-workers,[30] the hopping rate (which depends of the hopping electron probability and the atomic vibrational frequency) is maximized when the electron moves each time the local distortion patter, which is the same for the two sites involved. In this coincident effect, the phonon excitation assisting the electron jump occurs without introducing any further deformation. Alternatively, in the nonadiabatic regime, where $\alpha=\frac{3}{2}$ in Eq. (8), the electron jump probability is small (small values of the electron transfer integral). The electron has only a limited ability to follow the atomic motion.

Now, assuming the existence of small polarons in our system, we analyze the ρ behavior with both models described by Eq. (8) and the results are plotted in Fig. 8.

$$\rho = \rho_0 T^\alpha \exp\left[\frac{E_\rho}{k_B T}\right]. \tag{8}$$

With the nonadiabatic model, the activation energies are $E_\rho = 230$, 180, and 240 meV, for x=0, $\frac{1}{3}$, and 1 samples respectively (see Table II). The values obtained are close to those reported in similar vanadium spinels as MgV_2O_4 and ZnV_2O_4, i.e., approximately 200 meV (Ref. 16) and 130 meV in some manganites.[23,31]

Finally, in order to discuss the MR behavior in these inverted spinels, note that the observed phenomenon is completely different from the negative CMR that was extensively studied in the last years. In polycrystalline manganites oxides, the MR has been explained considering the combination of two mechanisms; one of them is predominant at low magnetic fields and is associated with the tunnel barriers between grains. This effect decreases with the increase in temperature, while, at high magnetic fields, an extra contribution is observed and is associated with the spin scattering with the FM domains aligned to the external magnetic field. Also, this effect is completely different from the common positive MR observed in the majority of metals due to the cyclotron orbits, which present very low values.

On the other hand, positive MR has been observed at high temperatures and is still not completely well understood in the spinel $Zn_{0.95}Cu_{0.05}Cr_2Se_4$,[32] where the thermal activation of carriers is the dominant mechanism. Although most other spinels contain vanadium, particularly in $MnTi_{2-x}V_xO_4$ with $x<1$, positive values in the MR were also observed. The authors explain this behavior as a Zeeman splitting of the conduction bands.[33] Also positive MR was observed in films of VO_x,[34] in pyrochlores structures $[Gd_2(Mo_{0.6}V_{0.4})_2O_7]$,[35] and transition metal doped ZnO films.[36] In this last system the phenomenon is explained invoking bound magnetic polarons, where thermodynamics fluctuations of the local magnetizations govern the hopping process.[37] Practically in all the cases mentioned, the systems present some type of magnetic order. However in our samples, we observed the phenomenon in the paramagnetic phase at high temperature far from the magnetic order transition. More recently similar behavior, high values of positive MR in a paramagnetic phase, has been found in organic materials, which has been explained in terms of hopping of polarons and formation of bipolarons in the presence of hyperfine fields (of the hydrogen nucleus, in our case, the manganese nucleus present hyperfine fields) and an external magnetic field.[38] Anyway, the origin of this positive MR that occurs in these spinels requires more detailed studies to clarify the correct mechanism involved.

IV. CONCLUSIONS

In summary, we presented the electrical transport and magnetic susceptibility data of $Mn_{2-x}V_{x+1}O_4$ ($x=0$, $\frac{1}{3}$, and 1) spinels. All the samples studied present semiconducting, positive MR and paramagnetic behavior associated with ferrimagnetic order at low temperature. Taking into account, the atomic positions obtained from the neutron powder diffraction Rietveld refinement and from the fit of the inverse magnetic susceptibility data, we propose the next ionic models

$$Mn^{2+}_{0.89}V^{3+}_{0.11}[Mn^{3+}_{1.11}Mn^{2+}_{0.11}V^{3+}_{0.89}]O_4,$$

$$Mn^{2+}_{1.00}[Mn^{2+}_{0.67}V^{3+}_{0.66}V^{4+}_{0.67}]O_4,$$

and

$$Mn^{2+}_{0.75}V^{3+}_{0.25}[Mn^{2+}_{0.25}V^{3+}_{0.175}]O_4$$

for $x=0$, $\frac{1}{3}$, and 1, respectively, to explain the magnetic properties.

We also found an important difference between the activation energies obtained from the Seebeck coefficient and electrical resistivity experiments. This difference is a clear indication that the predominant conduction mechanism is by small polarons. In particular these polarons are thermally activated in the non-adiabatic regime as it shows the best fit of the experimental resistivity data. Finally, one of the interesting properties founded in these inverse spinels is the high value of positive MR (>1%) at RT.

ACKNOWLEDGMENTS

R.E.C. and R.D.S. thank ANPCYT (Project Nos. PAV 22708, PICT 06-15102, and 21372) and CONICET (Grant No. PIP 5767/05). R.E.C. also thanks SECyT-UNC (Project No. 197/05). R.D.S. also thanks SECTyP-UNCu. E.V.P.M. and J.M.D thank CONICET for a fellowship. Also the authors thank C. A. Batista for the fruitful discussion.

[1] R. M. von Helmolt, J. Wecker, B. Holzapfel, L. Schultz, and K. Samwer, Phys. Rev. Lett. **71**, 2331 (1993).
[2] S. Jin, T. H. Tiefel, M. McCormack, R. A. Fastnacht, R. Ramesh, and L. H. Chen, Science **264**, 413 (1994).
[3] M. Viret, Lect. Notes Phys. **569**, 117 (2001) and references therein.
[4] C. Israel, M. Calderón, and N. D. Mathur, Mater. Today **10**, 24 (2007); R. D. Sánchez, J. Rivas, C. Vazquez-Vazquez, A. Lopez-Quintela, M. T. Causa, M. Tovar, and S. Oseroff, Appl. Phys. Lett. **68**, 134 (1996).
[5] C. N. R. Rao, A. Arulraj, A. K. Cheetham, and B. Raveau, J. Phys.: Condens. Matter **12**, R83 (2000).
[6] E. Dagotto, *Nanoscale Phase Separation and Colossal Magnetoresistance*_(Springer, Germany, 2003); See also E. Dagotto, T. Hotta, and A. Moreo, Phys. Rep. **344**, 1 (2001) and references therein.
[7] M. Fäth, S. Freisem, A. A. Menovsky, Y. Tomioka, J. Aarts, and J. A. Mydosh, Science **285**, 1540 (1999); J. M. De Teresa, M. R. Ibarra, P. A. Algarabel, C. Ritter, C. Marquina, J. Blasco, J. Garcia, A. del Moral, and Z. Arnold, Nature (London) **386**, 256 (1997).
[8] A. J. Millis, Phys. Rev. B **53**, 8434 (1996); A. J. Millis, P. B. Littlewood, and B. I. Shraiman, Phys. Rev. Lett. **74**, 5144 (1995).
[9] M. Jaime, M. B. Salamon, M. Rubinstein, R. E. Treece, J. S. Horwitz, and D. B. Chrisey, Phys. Rev. B **54**, 11914 (1996).
[10] H. Tsunetsugu and Y. Motome, Phys. Rev. B **68**, 060405(R) (2003); Y. Motome and H. Tsunetsugu, Physica B **359–361**, 1222 (2005).
[11] O. Tchernyshyov, Phys. Rev. Lett. **93**, 157206 (2004).
[12] S. Di Matteo, G. Jackeli, and N. B. Perkins, Phys. Rev B **72**, 020408(R) (2005).
[13] T. Maitra and R. Valentí, Phys. Rev. Lett. **99**, 126401 (2007).
[14] J. E. Greedan, J. Mater. Chem. **11**, 37 (2001) and references therein.
[15] M. Onoda, and J. Hasegawa, J. Phys.: Condens. Matter **15**, L95 (2003).
[16] H. Mamiya and M. Onoda, Solid State Commun. **95**, 217 (1995).
[17] N. Tristan, J. Hemberger, A. Krimmel, H. A. Krug von Nidda, V. Tsurkan, and A. Loidl, Phys. Rev. B **72**, 174404 (2005).
[18] R. Plumier and M. Sougi, Physica B **155**, 315 (1989).
[19] R. Plumier and M. Sougi, Solid State Commun. **64**, 53 (1987).
[20] K. Adachi, T. Suzuki, K. Kato, K. Osaka, M. Takata, and T. Katsufuji, Phys. Rev. Lett. **95**, 197202 (2005).
[21] E. V. Pannunzio-Miner, J. M. De Paoli, R. D. Sánchez, and R. E. Carbonio, Mater. Res. Bull. **44**, 1586 (2009).
[22] V. O. Garlea, R. Jin, D. Mandrus, B. Roessli, Q. Huang, M. Miller, A. J. Schultz, and S. E. Nagler, Phys. Rev. Lett. **100**, 066404 (2008).
[23] M. F. Hundley and J. J. Neumeier, Phys. Rev. B **55**, 11511 (1997).
[24] P. M. Chaikin and G. Beni, Phys. Rev. B **13**, 647 (1976).
[25] S. Blanco-Canosa, F. Rivadulla, V. Pardo, D. Baldomir, J. S. Zhou, M. García-Hernandez, M. A. López-Quintela, J. Rivas, and J. B. Goodenough, Phys. Rev. Lett. **99**, 187201 (2007).
[26] A. J. Bosman and H. J. van Daal, Adv. Phys. **19**, 1 (1970).
[27] D. Niebieskikwiat and R. D. Sánchez, J. Magn. Magn. Mater. **221**, 285 (2000).
[28] J. Lago, P. D. Battle, M. J. Rosseinsky, A. I. Coldea, and J. Singleton, J. Phys.: Condens. Matter **15**, 6817 (2003).
[29] J. B. Goodenough, Mater. Res. Bull. **5**, 621 (1970).
[30] M. Jaime, H. T. Hardner, M. B. Salamon, M. Rubinstein, P. Dorsey, and D. Emin, Phys. Rev. Lett. **78**, 951 (1997).
[31] M. Jaime, M. B. Salamon, K. Petit, M. Rubinstein, R. E. Treece, J. S. Horowitz, and D. B. Chrisey, Appl. Phys. Lett. **68**, 1576 (1996).
[32] Y. Onose, N. Takeshita, C. Terakura, H. Takagi, and Y. Tokura, Phys. Rev. B **72**, 224431 (2005).
[33] T. Sonehara, K. Kato, K. Osaka, M. Takata, and T. Katsufuji, Phys. Rev. B **74**, 104424 (2006).
[34] A. D. Rata, V. Kataev, D. Khomskii, and T. Hibma, Phys. Rev. B **68**, 220403(R) (2003).
[35] I. O. Troyanchuk, N. V. Kasper, D. D. Khalyavin, H. Szymczak, and A. Nabialek, Phys. Status Solidi A **167**, 151 (1998).
[36] J. Wang, Z. Gu, M. Lu, D. Wu, C. Yuan, S. Zhang, Y. Chen, S. Zhu, and Y. Zhu, Appl. Phys. Lett. **88**, 252110 (2006).
[37] A. G. Petukhov and M. Foygel, Phys. Rev. B **62**, 520 (2000).
[38] P. A. Bobbert, T. D. Nguyen, F. W. A. vanOost, B. Koopmans, and M. Wohlgenannt, Phys. Rev. Lett. **99**, 216801 (2007).